# Zooming in on quasar accretion

**David Floyd**

AAO & University of Melbourne

**email: dfloyd@unimelb.edu.au**

Gravitational microlensing provides information at microarcsecond scales through the detection of the imperfections in the lensing system (stars in a lensing galaxy). Applied to quasars this provides valuable physical detail on the central engine. We have developed the technique to use single epoch images to constrain accretion mechanisms and explore the physical structure of the central engine, just a few light days across. Using broad-band imaging, we place the strongest constraints on the size of the emission region to date, and interesting constraints on the accretion mechanism. There is mounting evidence that the Shakura-Sunyaev [SS73] mechanism is unable to account for the observed temperature profile in quasar accretion discs, and ongoing spectroscopic studies with Magellan, Gemini and VLT will finally open the central light week of quasars to detailed scrutiny.

## Lensing and Microlensing Background

Images form at turning points (min, max, saddle) in light travel-time "surface".

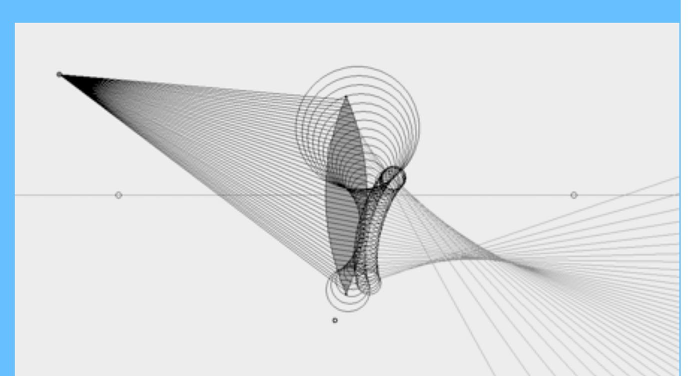

Magnification, μ at a point on source plane is described by convergence, κ and shear, γ, which change slowly with position across the plane:

$$\mu = \frac{1}{[(1-\kappa_{tot})+\gamma][(1-\kappa_{tot})-\gamma]} \begin{cases} 1-\kappa_{tot}-\gamma>0 & \text{(Min)} \\ 1-\kappa_{tot}-\gamma<0 & \text{(Saddle)} \\ 1-\kappa_{tot}+\gamma<0 & \text{(Max)} \end{cases}$$

**N.B.: Saddle point images can be demagnified wrt minima!**

Microlensing (due to gravitational substructure in lens - stars, CDM) introduces perturbations in travel-time surface and thus in magnification -> **Magnication maps [B+07, SW02]**

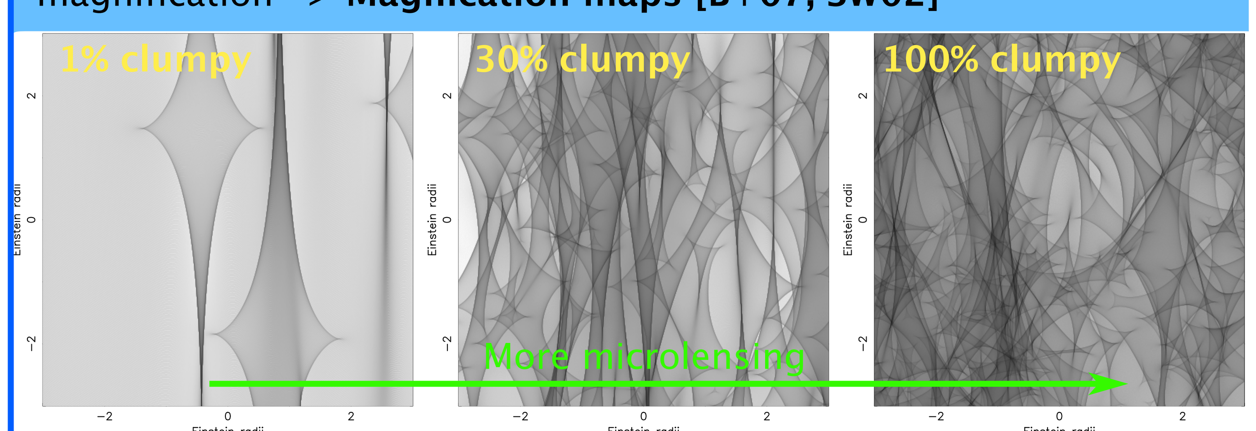


**Above: Magnification (grey-scale) maps** with source position for a simulated microlens population (stars in a galaxy). These are like the caustics that appear on the bottom of a swimming pool. Darker areas correspond to regions of higher magnification. Microlensing (like ripples in a pool) creates a complicated travel-time surface.

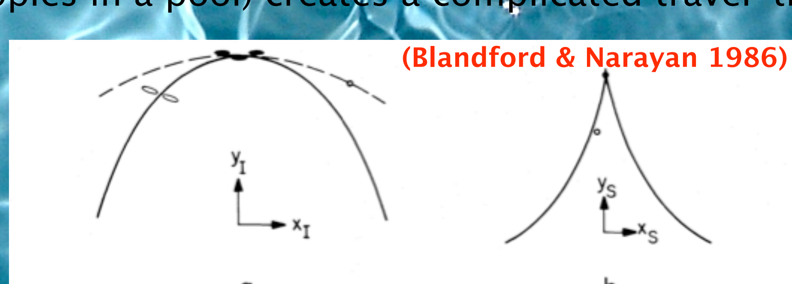


**Above: Caustics** on the source plane (b) separate minimum and saddle point images in the image plane (a). In the absence of microlensing, nearby images have similar magnification (κ and γ are similar). But in a microlensed system, we may observe strong differential magnification between a close image pair.

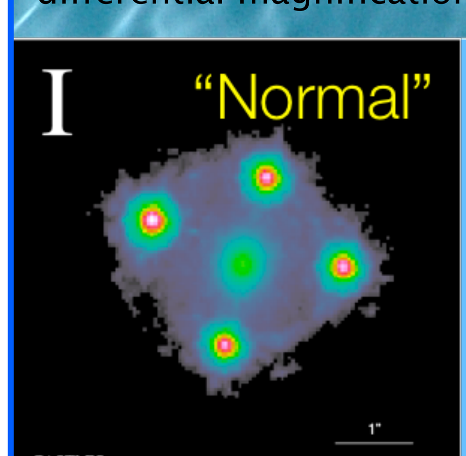


An anomaly (right) may be caused by gravitational microlensing, millilensing, dust absorption or variability. See below for microlensing explanation.

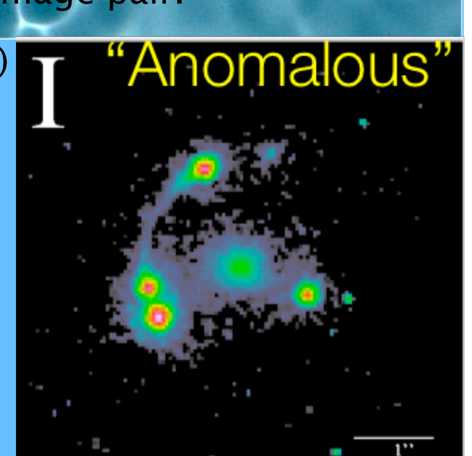


8/10 lensed QSO's with close image pairs exhibit an anomalously dim saddle point image in the X-ray, with a 4% chance of occurring at random [Pooley+07, F+09].

**Microlensing Magnification Probability Distributions:**

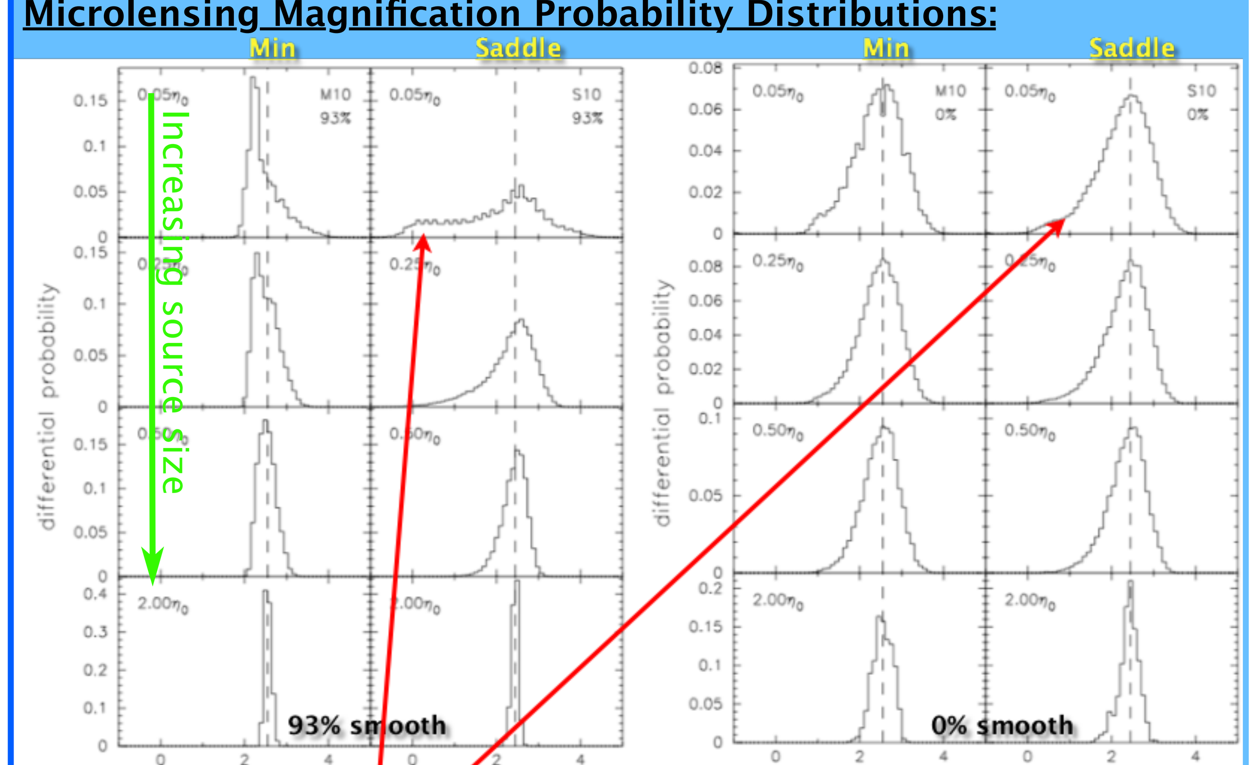


**Anomalies occur when saddlepoint image is only weakly magnified relative to min image.**

## Lensed Quasars

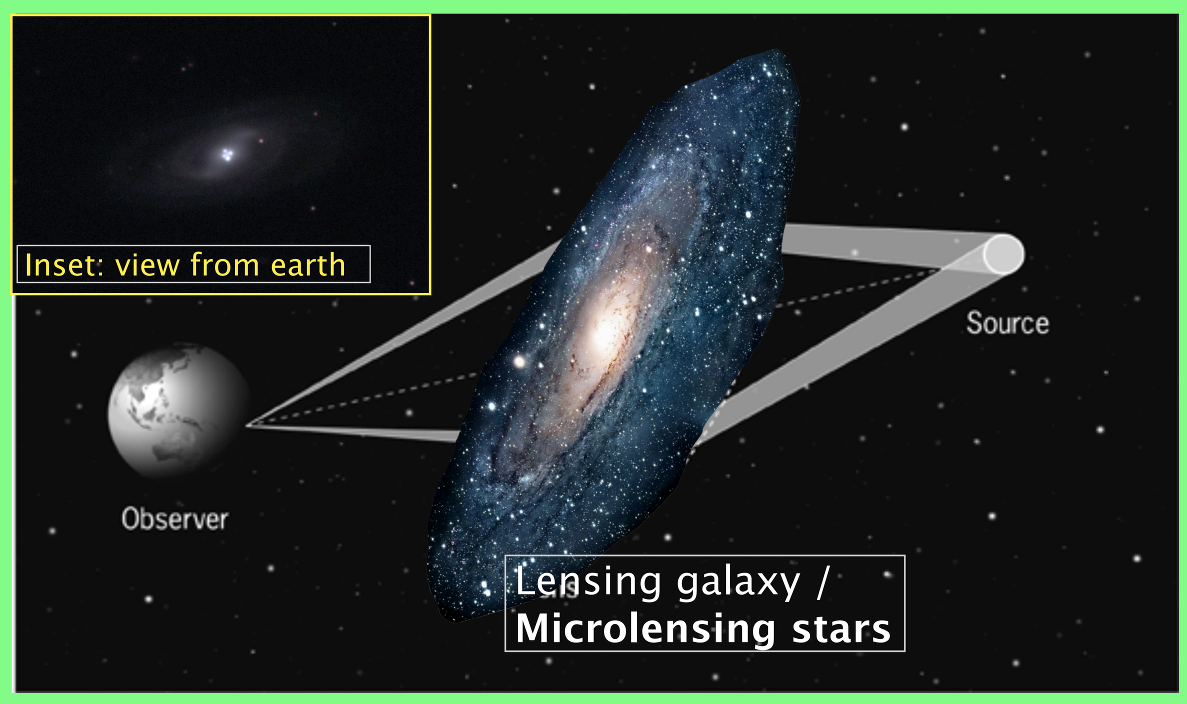


**Below:** Magellan [F+09] & HST (CASTLES) imaging of the quadruple lensed quasar, **SDSS J0924+0219**. This is the most anomalous known quasar (see "A" and "D" in image below). It exhibits strong optical variability, is radio-quiet, and is found at a redshift of $z_s$=1.524. The lens is at $z_l$ = 0.394. See also [B+08].

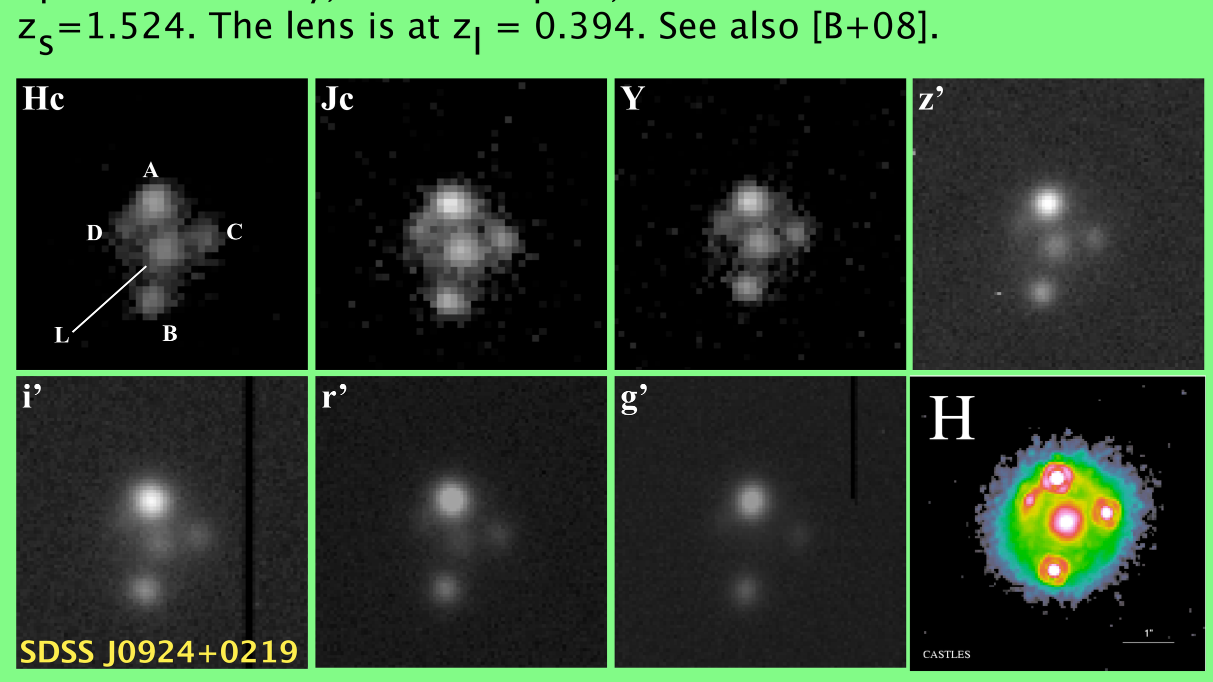


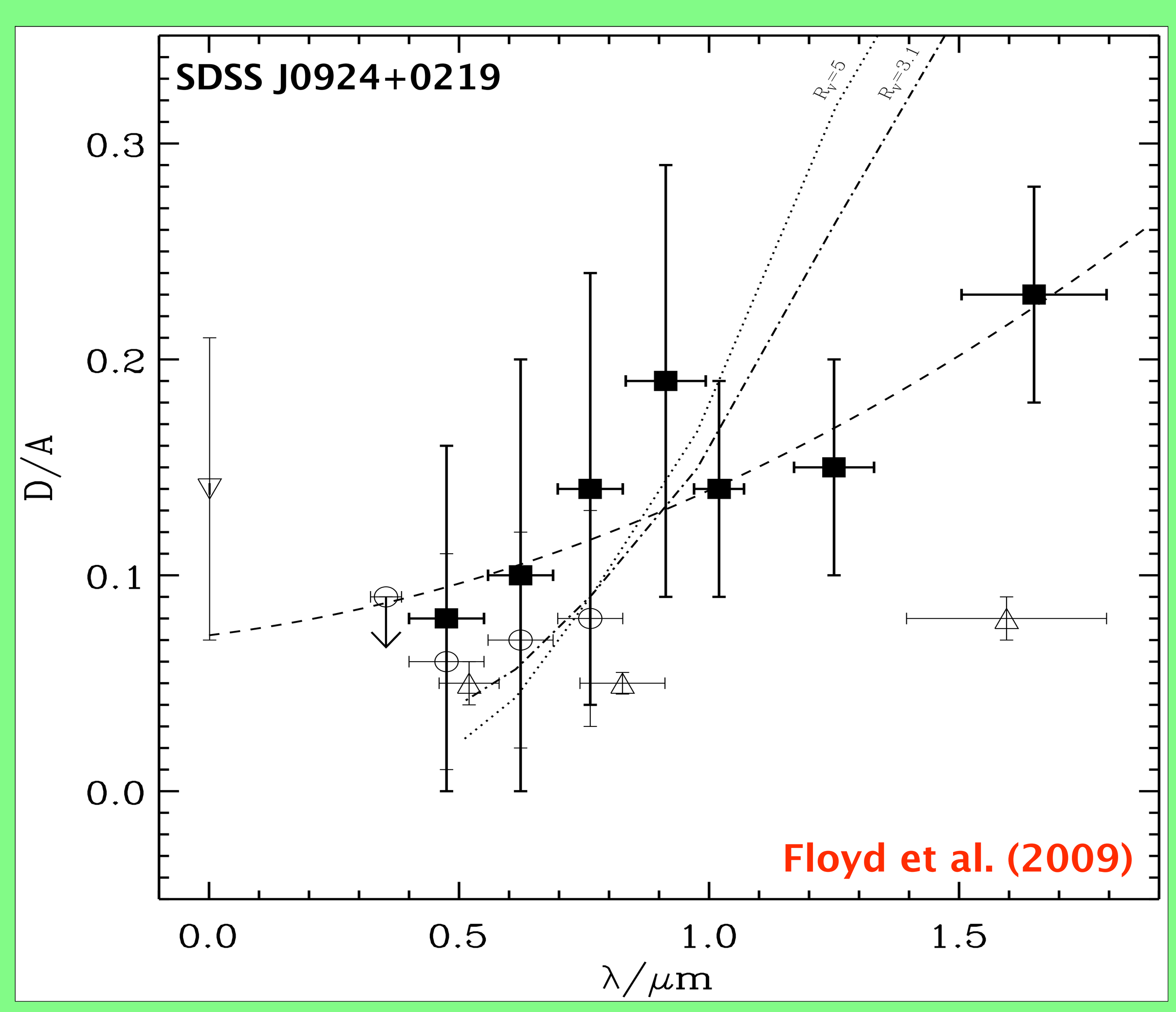


**Above:** The flux ratio of image D to A with wavelength. Gravitational macrolensing predicts D/A~1. The filled squares represent a single epoch of Magellan data, with older multi-epoch data represented by circles [Inada+03]; triangles [Keeton +06]; down-pointing triangle [Pooley+07]. Dust models (dotted, dot-dashed lines; [Mathis 1990]) are incapable of explaining the observed slope. Millilensing can help explain the strongly anomalous NIR flux ratio, but cannot explain the slope. Microlensing offers the only explanation of the observed wavelength-dependence, and implies that we are observing a source that gets smaller as we move blueward, as expected for any accretion disk model. By exploring the slope we can constrain accretion disc models.

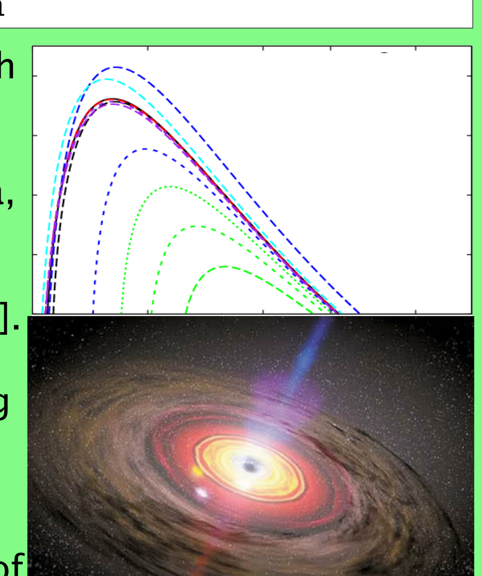

**T(r) ~ r^p**
**λ(r) ~ r^ζ**
**[BB:ζ=1/p]**

**Accretion disk models:** A range of models exist to describe how angular momentum is transported outwards in an accretion disc. Most are based on the α-disk prescription [SS73], but MRI models [e.g. Agol & Krolik 2000] predict a steeper temperature profile.

## Results

**Top panel:** joint probability distributions for the radius of the u′-band emission region, $\sigma_0$ and the power-law index, ζ (contours: 1σ, 2σ, 3σ). The dashed lines illustrate four accretion disc models. The small circle indicates the location of the maximum in the probability distribution.

**Bottom panel:** cumulative probability distributions for $\sigma_0$ (left) and ζ (right).

**All α-disk models are excluded at the >2σ level, with a steeper temperature profile (e.g. MRI) preferred.**

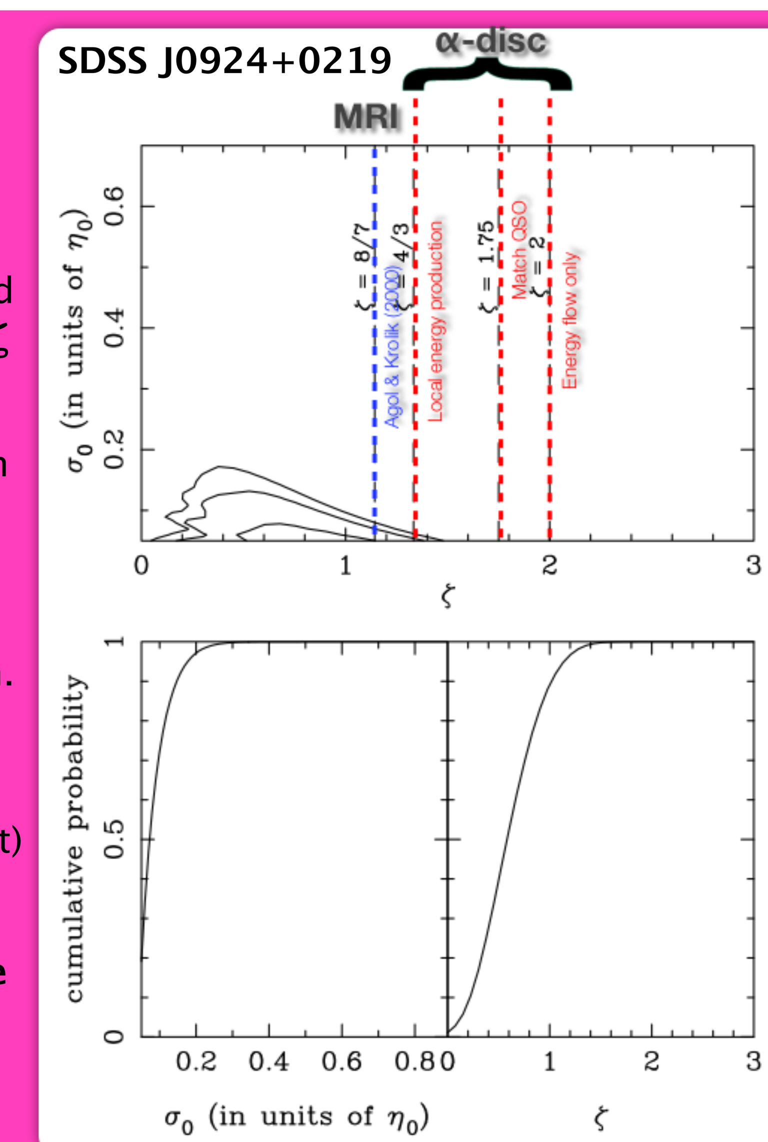


## Future work

Work using broad-band photometry is biased by the presence of broad lines in each bandpass (emitted at different radii to the equivalent wavelength continuum photons and will therefore have differing microlens signatures). We have begun to explore the structure of the accretion disk and BELR independently, using IFU spectra (GMOS, X-shooter, IMACS). We have obtained VLT X-shooter spectra of 2 targets (Floyd et al. in prep). Higher resolution spectroscopy can explore the detailed structure of BELR line emission, to constrain outflow and wind models (see below).

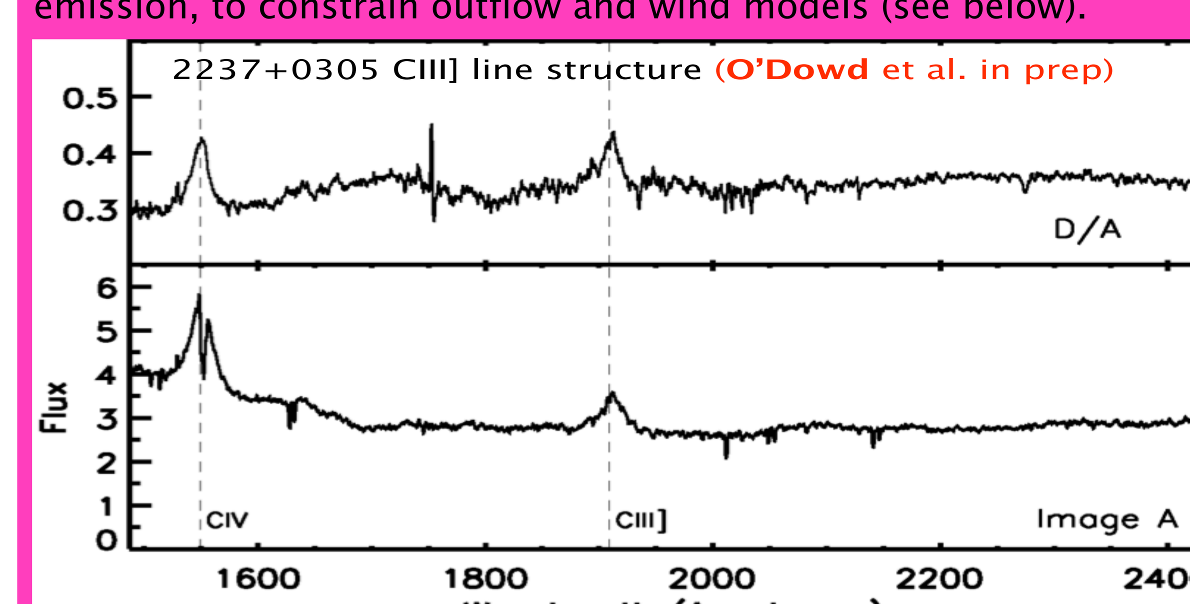


Comparing spectroscopic results with CLOUDY (Ferland +98) photoionization simulations of line emission, allows us to explore the detailed physics of emission in the central engine (below).

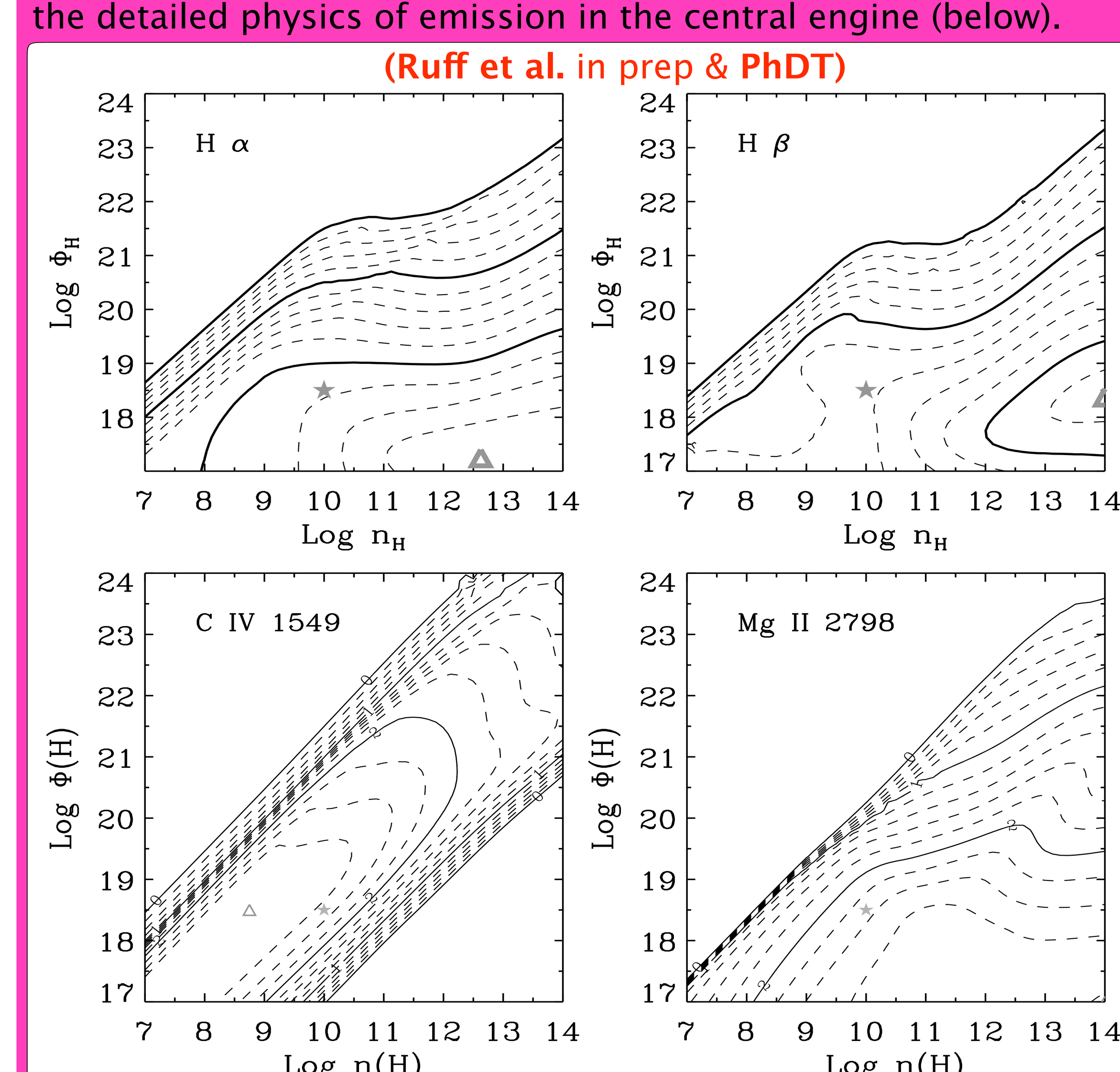


**Microlensing is complementary to reverberation mapping, works at far higher redshifts, and provides a more universal scale measurement (no variability required). We are finally entering a truly scientific era for the study of quasar emission!**

## References

Agol & Krolik 2000, ApJ, **528**, 161
B+07: Bate, Webster & Wyithe 2007, MNRAS, **381**, 1591
B+08: Bate, Floyd, Webster & Wyithe 2008, MNRAS, **391**, 1955
Blandford & Narayan 1986, ApJ, **310**, 568
F+09: Floyd et al 2009, MNRAS, **398**, 233
Ferland et al. 1998, PASP, **110**, 761
Inada et al. 2003, AJ, **126**, 666
Keeton et al. 2006, ApJ, **639**, 1
Mathis 1990, ARA&A, **28**, 37
**SS73:** Shakura & Sunyaev 1973, A&A, **24**, 337
**SW02:** Schechter & Wambsganss 2002, ApJ, **580**, 685
Pooley et al. 2007, ApJ, **661**, 19